

# Phenomenology of $E_6$ -Inspired Leptophobic $Z'$ Boson at the LHC

Cheng-Wei Chiang,<sup>1,2,3,\*</sup> Takaaki Nomura,<sup>4,†</sup> and Kei Yagyu<sup>1,‡</sup>

<sup>1</sup>*Department of Physics and Center for Mathematics and Theoretical Physics,  
National Central University, Chungli, Taiwan 32001, ROC*

<sup>2</sup>*Institute of Physics, Academia Sinica, Taipei, Taiwan 11529, ROC*

<sup>3</sup>*Physics Division, National Center for Theoretical Sciences, Hsinchu, Taiwan 30013, ROC*

<sup>4</sup>*Department of Physics, National Cheng Kung University,  
1, Ta-Hsueh Road, Tainan, Taiwan 70101, ROC*

## Abstract

We study collider phenomenology of a leptophobic  $Z'$  boson existing in eight scenarios of the  $E_6$  grand unified theory, differing in particle embedding. When the  $Z'$  boson is kinematically allowed to decay into a pair of top quarks, most scenarios have a lower bound of about 1 TeV on the  $Z'$  mass  $m_{Z'}$  based upon current LHC data for the  $pp \rightarrow t\bar{t}$  process for the collision energy of 8 TeV and an integrated luminosity of  $19.6 \text{ fb}^{-1}$ . We investigate the photon associated production of the  $Z'$  boson, followed by the decay of a pair of bottom quark decays,  $pp \rightarrow \gamma Z' \rightarrow \gamma b\bar{b}$ , to constrain the lower mass region  $m_{Z'} < 2m_t$ . We compute the expected significance of signal events as a function of  $m_{Z'}$  in the lower mass region based on the current LHC data. A projection of required luminosity for a higher signal significance at the 14-TeV LHC is also estimated.

PACS numbers: 12.60.Cn, 14.70.Hp

---

\*Electronic address: chengwei@ncu.edu.tw

†Electronic address: nomura@ncu.edu.tw

‡Electronic address: keiyagyu@ncu.edu.tw

## I. INTRODUCTION

The operation of the 7- and 8-TeV runs of the CERN Large Hadron Collider (LHC) has provided us with quite important information about electroweak symmetry breaking; namely, the discovery of a standard model (SM)-like Higgs boson [1] with the mass of about 126 GeV. This fact becomes a strong guideline for us to consider various models beyond the SM. Moreover, null results of any other new particles so far impose lower bounds on their masses and/or new physics scales. It is of great interest to discuss what kind of signals from new physics can be expected at the upcoming 13- and 14-TeV runs, while taking into account the data collected in the 8-TeV run.

An extra  $U(1)$  gauge symmetry is often introduced based on various motivations in physics beyond the SM, resulting in an additional massive neutral gauge boson usually called the  $Z'$  boson. For example, there are usually additional  $U(1)$  gauge symmetries in grand unified theories (GUT's) such as the  $E_6$  model [2]. Besides, the discrete  $Z_2$  symmetry required for stabilizing dark matter candidates can naturally emerge from a local  $U(1)$  gauge group [3–5]. An extra  $U(1)$  has also been employed in supersymmetric models [6] (so-called UMSSM) to facilitate a strong first order electroweak phase transition, as required to realize successful electroweak baryogenesis [7]. Properties of such  $Z'$  bosons strongly depend on the origin of the corresponding  $U(1)$  symmetry in models. Therefore, phenomenological studies of  $Z'$  bosons are essential to distinguish such new physics models [8].

Searches for  $Z'$  bosons have been performed mainly using the dilepton events at the LHC. If the couplings of the  $Z'$  boson with fermions are the same as those of the  $Z$  boson, the lower mass limit has been found to be 2.86 TeV (1.90 TeV) at the 95% confidence level from collisions at 8 TeV with an integrated luminosity of  $19.5 \text{ fb}^{-1}$  by using  $e^+e^-$  and  $\mu^+\mu^-$  [9] ( $\tau^+\tau^-$  [10]) events.

However, such a search becomes ineffective when the  $Z'$  boson does not couple to the leptons. In this paper, we focus on the study of leptophobic  $Z'$  bosons derived from different scenarios of the  $E_6$  GUT. In the  $E_6$  model [11], there is kinetic mixing between the  $U(1)_Y$  group and the extra  $U(1)$ 's after GUT breaking. As a result, the  $Z'$  charge of each fermion is a linear combination of these  $U(1)$  charges, involving two free parameters. These two degrees of freedom can be chosen so that the  $Z'$  charges for the left-handed lepton and right-handed charged lepton are zero, rendering the leptophobia nature.

Phenomenological studies of the leptophobic  $Z'$  boson had been done in Refs. [12, 13, 16, 17], with collider signals for the  $Z'$  searched for at the Tevatron [12, 13] and the LHC [13]. LHC collider signatures of a leptophobic  $Z'$  boson that couples to a dark matter candidate had been studied in

Refs. [14]. In Refs. [15, 16], a leptophobic  $Z'$  boson with the mass of about 150 GeV was proposed to explain the excess in the  $Wjj$  events observed by the Tevatron CDF Collaboration. Effects of the leptophobic  $Z'$  to the  $e^+e^- \rightarrow q\bar{q}$  process due to the  $Z$ - $Z'$  mixing had been analyzed in Ref. [17].

In this paper, we discuss all possible scenarios of the leptophobic  $Z'$  boson in the  $E_6$  GUT model, differing in the  $Z'$  charges of fermions due to different particle embeddings [18]. We consider the bound on the  $Z'$  mass according to the current collider experiments. Most of the scenarios can be excluded by the  $pp \rightarrow Z' \rightarrow t\bar{t}$  process up to about  $\mathcal{O}(1)$  TeV by the current LHC data. However, when the  $Z'$  mass is below the threshold for the decay into a pair of top quarks, such a method does not apply. We thus consider the light  $Z'$  boson scenario by concentrating on the  $pp \rightarrow Z'\gamma \rightarrow b\bar{b}\gamma$  process.

The structure of this paper is as follows. We review the interaction Lagrangian for the leptophobic  $Z'$  boson in Section II, where the decay and production of the  $Z'$  are also discussed. The current experimental bound on the  $Z'$  mass is analyzed in Section III. In Section IV, we perform a simulation study for the  $pp \rightarrow Z'\gamma \rightarrow b\bar{b}\gamma$  process particularly for the case of a light  $Z'$ . Our findings are summarized in Section V. A brief review of the different leptophobic scenarios in the  $E_6$  model is given in the Appendix.

## II. LEPTOPHOBIC $Z'$ BOSON

The interactions of the leptophobic  $Z'$  boson with SM quarks are given by

$$\mathcal{L} = \sum_{q=u,d} g_{Z'} \bar{q} \gamma^\mu (v_q - \gamma_5 a_q) q Z'_\mu, \quad (1)$$

where  $u$  and  $d$  represent the up- and down-type quarks, respectively. For simplicity, we assume no or at least negligible flavor-changing couplings. The vector coupling coefficient  $v_q$  and the axial-vector coupling coefficient  $a_q$  are related to the  $Z'$  charge  $\bar{Q}_f$  of the quark  $q$  by

$$v_q = \frac{\bar{Q}_Q}{2} \left( 1 + \frac{\bar{Q}_q}{\bar{Q}_Q} \right), \quad a_q = \frac{\bar{Q}_Q}{2} \left( 1 - \frac{\bar{Q}_q}{\bar{Q}_Q} \right), \quad (\text{for } q = u, d). \quad (2)$$

Appendix briefly reviews the scenarios in the  $E_6$  GUT model that realize leptophobia for the  $Z'$  boson, along with the corresponding  $Z'$  charges  $\bar{Q}_f$  given in Table IV. We note here that the value of the gauge coupling constant  $g_{Z'}$  can be predicted at the TeV scale according to renormalization group running from the GUT scale, which depends on the details of matter contents and unification scale. Nevertheless, we adopt  $g_{Z'} = \sqrt{5/3}g'$ , as in Ref. [19], for phenomenological analyses.

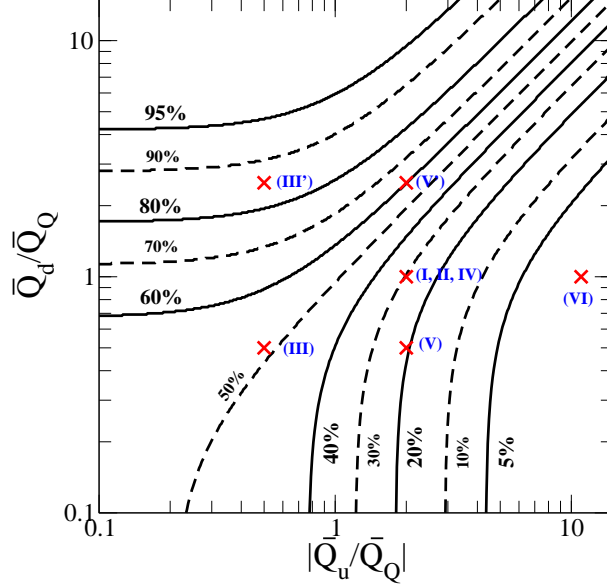


FIG. 1: Contour plot of the total branching fraction for the  $Z'$  decaying into the down-type quarks on the  $|\bar{Q}_u/\bar{Q}_Q|$  and  $\bar{Q}_d/\bar{Q}_Q$  plane in the case of  $m_{Z'} = 1$  TeV. The predictions for the scenarios defined in Table IV in Appendix are indicated by the red crosses.

The decay rate of  $Z'$  into a quark pair is

$$\begin{aligned} \Gamma(Z' \rightarrow q\bar{q}) &= g_{Z'}^2 \frac{m_{Z'}}{4\pi} [v_q^2(1 + 2x_q) + a_q^2(1 - 4x_q)] \sqrt{1 - 4x_q} \\ &= g_{Z'}^2 \frac{m_{Z'}}{4\pi} \frac{\bar{Q}_Q^2}{2} \left[ 1 + \left( \frac{\bar{Q}_q}{\bar{Q}_Q} \right)^2 - x_q \left( 1 - \frac{\bar{Q}_q}{\bar{Q}_Q} \right)^2 \right] \sqrt{1 - 4x_q}, \quad \text{with } x_q = \frac{m_q^2}{m_{Z'}^2}. \end{aligned} \quad (3)$$

Apart from  $x_q$  that depends on the  $Z'$  mass, the terms inside the square brackets involve just the two  $Z'$  charge ratios,  $\bar{Q}_u/\bar{Q}_Q$  and  $\bar{Q}_d/\bar{Q}_Q$ . Among the eight scenarios given in Table IV, Scenario-I and Scenario-IV have the same  $Z'$  charge, and Scenario-II have the same charge ratios as them, so that the decay branching fractions are the same in these three scenarios. However, the total width and the production cross section for  $Z'$  can be different between Scenario-I or Scenario-IV and Scenario-II as they are controlled by the overall  $\bar{Q}_Q$  factor. Therefore, the number of distinct scenarios is effectively reduced down to six. In the following, we only present the results for Scenario-I with the understanding that those for Scenario-II and Scenario-IV can be obtained by appropriate scaling. Notice that the decay rate depends little on the sign of  $Z'$  charge in the limit of  $x_q \rightarrow 0$ .

In Fig. 1, we show the contour plot of the total branching fraction for the  $Z'$  decaying into a pair of down-type quarks,  $\sum_{q=d,s,b} \mathcal{B}(Z' \rightarrow q\bar{q})$ , on the  $|\bar{Q}_u/\bar{Q}_Q|$  and  $\bar{Q}_d/\bar{Q}_Q$  plane, taking  $m_{Z'} = 1$  TeV as an example. The reason we use the absolute value of  $\bar{Q}_u/\bar{Q}_Q$  as the horizontal axis is simply

Scenario	$u\bar{u}$ [%]	$t\bar{t}$ [%]	$d\bar{d}$ [%]	width [GeV]
Scenario-I				3.2, 7.2, 11.1
Scenario-II	27.6, 24.7, 24.2	11.8, 20.8, 22.5	11.0, 9.9, 9.7	0.32, 0.72, 1.1
Scenario-IV				3.2, 7.2, 11.1
Scenario-III	18.4, 17.1, 16.9	7.9, 14.4, 15.7	18.4, 17.1, 16.9	0.73, 1.6, 2.4
Scenario-III'	5.0, 4.9, 4.9	2.2, 4.2, 4.6	29.3, 28.7, 28.5	2.7, 5.4, 8.2
Scenario-V	31.5, 27.8, 27.2	13.5, 23.5, 25.3	7.9, 7.0, 6.8	1.7, 3.9, 5.9
Scenario-V'	14.8, 13.9, 13.7	6.3, 11.7, 12.8	21.4, 20.2, 19.9	3.6, 7.7, 11.7
Scenario-VI	37.9, 34.0, 33.3	22.3, 30.4, 31.7	0.6, 0.6, 0.5	5.7, 12.8, 19.6

TABLE I: Branching fractions and total width of  $Z'$  in the scenarios listed in Table IV. The column for  $u\bar{u}$  ( $d\bar{d}$ ) displays the branching fractions for  $Z' \rightarrow u\bar{u}$  and  $Z' \rightarrow c\bar{c}$  ( $Z' \rightarrow d\bar{d}$ ,  $Z' \rightarrow s\bar{s}$  and  $Z' \rightarrow b\bar{b}$ ). The three numbers in each entry are the predicted for  $m_{Z'} = 500$  GeV, 1000 GeV and 1500 GeV, respectively.

because  $\bar{Q}_u$  is always negative among the scenarios. The predictions for the various leptophobic scenarios are indicated by red crosses. The maximum (about 85%) and the minimum (less than 5%) are realized in Scenario-III' and Scenario-VI, respectively. Note that varying the  $Z'$  mass will cause shifts in the contours as a result of the third term in the square brackets of Eq. (3). The general tendency is that the total down-quark branching fraction becomes smaller for larger  $Z'$  mass, as reflected in Table I, where the branching fraction of each mode and the total width are computed for  $m_{Z'} = 500$ , 1000 and 1500 GeV.

In the following discussions, we will concentrate on the six scenarios that present distinct branching fraction patterns of the  $Z'$ , *i.e.*, Scenario-I, Scenario-III, Scenario-III', Scenario-V, Scenario-V', and Scenario-VI.

Next, we discuss dominant processes for producing the  $Z'$  at the LHC. There are the  $s$ -channel  $pp \rightarrow Z'$  process and the  $t$ -channel  $pp \rightarrow Z'V$  ( $V = \gamma, Z$  and  $W^\pm$ ) process of associated production. We calculate the production cross sections for these processes and those in the subsequent analyses with the help of CalcHEP [20] package and using CTEQ6L for the parton distribution functions (PDF's). In Fig. 2, the  $s$ -channel production cross section is shown as a function of  $m_{Z'}$  for the collision energy of 8 TeV (left panel) and 14 TeV (right panel). The biggest (smallest) cross section in the whole mass range is given by Scenario-VI (Scenario-III), because of the larger (smaller)  $\bar{Q}_u$  charge for the up-type quarks.

In Fig. 3, the associated production cross sections for the  $pp \rightarrow Z'\gamma$ ,  $pp \rightarrow Z'Z$  and  $pp \rightarrow Z'W$  processes are shown as a function of  $m_{Z'}$  by the black, red and blue curves, respectively, also for the

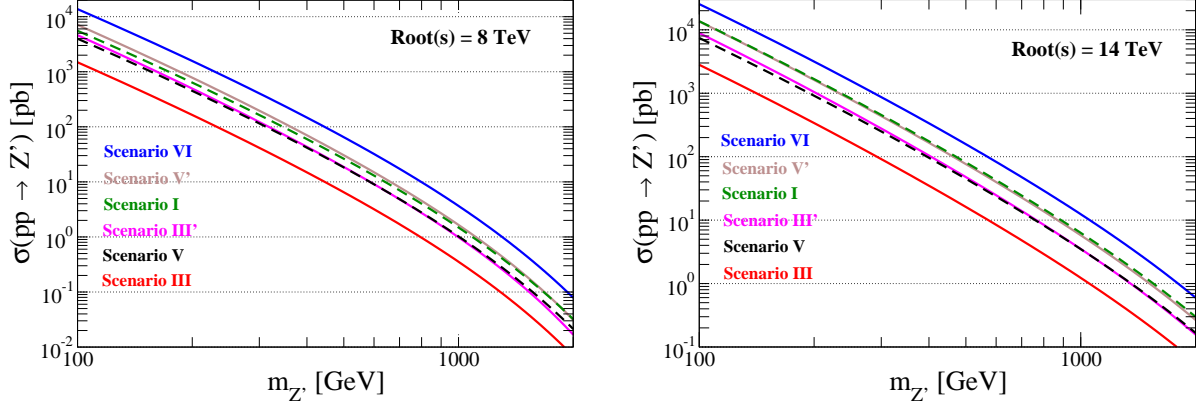


FIG. 2: Production cross sections of the  $pp \rightarrow Z'$  process as a function of  $m_{Z'}$  for the collision energy of 8 TeV (left) and 14 TeV (right) in the six scenarios.

collision energy of 8 TeV (dashed curves) and 14 TeV (solid curves). For the  $pp \rightarrow Z'W$  process, the  $W^+$  and  $W^-$  contributions are summed over. We impose the  $p_T(\gamma) > 10$  GeV cut for the  $pp \rightarrow Z'\gamma$  process to avoid collinear singularity of the produced photon, where  $p_T(\gamma)$  denotes the transverse momentum for the photon. In most cases, the cross sections are generally ranked in the order of  $Z'\gamma$ ,  $Z'W$  and  $Z'Z$  except for Scenario-VI. In the large  $m_{Z'}$  region, the produced vector boson tends to get smaller transverse mass, so that the production cross section of  $Z'\gamma$  reduces faster than those of  $Z'Z$  and  $Z'W$ , as a result of the  $p_T(\gamma)$  cut.

### III. CONSTRAINTS ON THE $Z'$ MASS BY CURRENT DATA

In this section, we discuss various constraints on the  $Z'$  mass in the six scenarios. We consider the current data on the  $pp \rightarrow Z' \rightarrow t\bar{t}$  and dijet processes at the LHC, as well as the  $Z'\bar{q}q$  couplings extracted from UA2 experiment.

#### A. The $pp \rightarrow t\bar{t}$ process

The upper limit at 95% confidence level (CL) for the cross section of  $pp \rightarrow t\bar{t}$  has been reported using the  $19.6 \text{ fb}^{-1}$  data at 8 TeV in Ref. [21]. This limit can be converted into a constraint on  $m_{Z'}$  because of the  $pp \rightarrow Z' \rightarrow t\bar{t}$  process.

In Fig. 4, the cross section of  $pp \rightarrow Z' \rightarrow t\bar{t}$  process is shown as a function of  $m_{Z'}$  with the help of CalcHEP [20] package and using the CTEQ6L PDF's. The dashed curve corresponds to the experimental upper limit for the cross section at the 95% CL, where the narrow width assumption

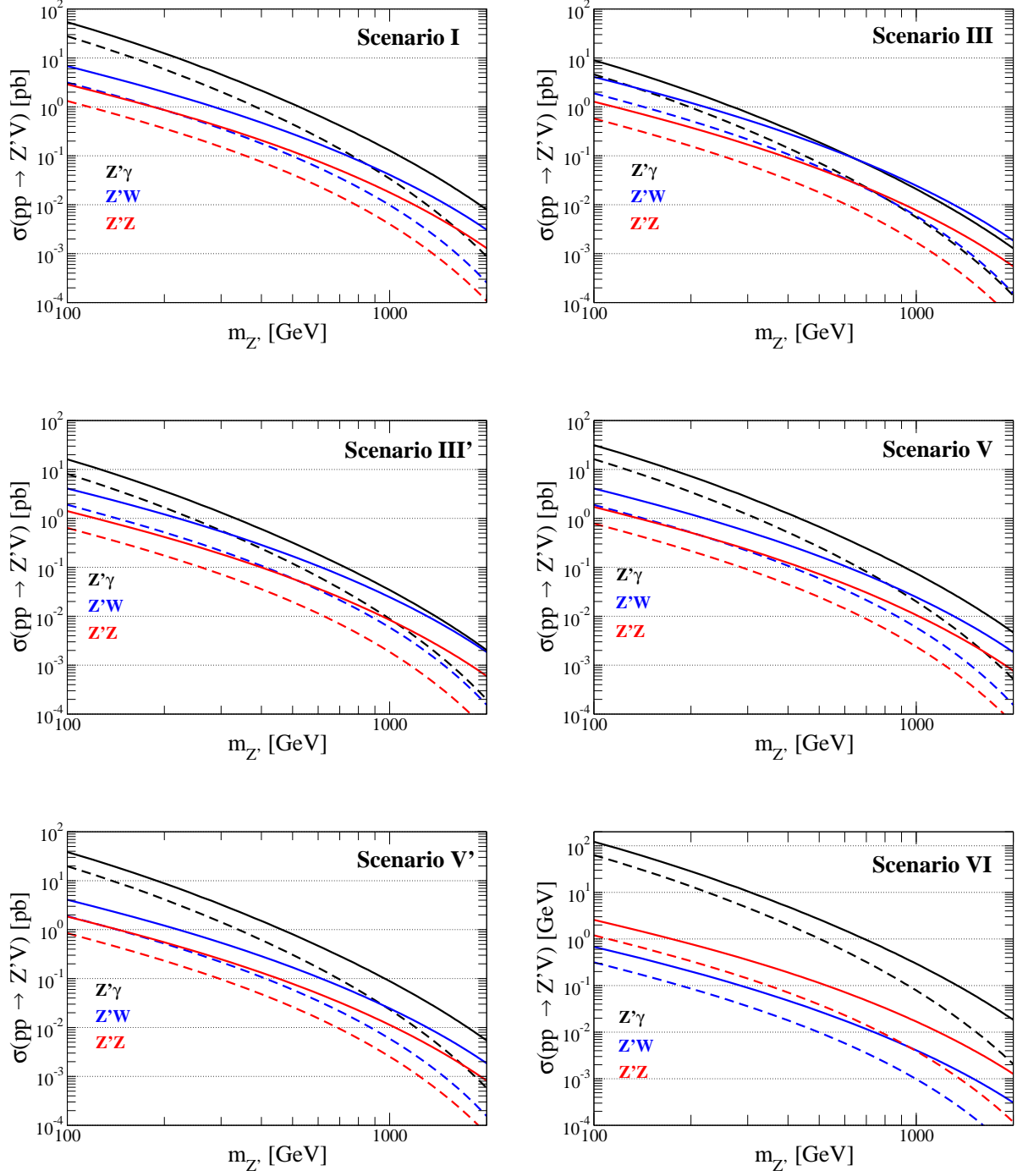


FIG. 3: Cross sections of the  $pp \rightarrow Z'V$  ( $V = \gamma, Z$  and  $W^\pm$ ) process as a function of  $m_{Z'}$  for the collision energy of 8 TeV (dashed curves) and 14 TeV (solid curves). For the  $pp \rightarrow Z'\gamma$  process, we impose  $p_T(\gamma) > 10$  GeV to avoid the collinear singularity.

is employed; *i.e.*,  $\Gamma_{Z'}/m_{Z'} = 1.2\%$  with  $\Gamma_{Z'}$  denoting the total width of  $Z'$ . In Scenario-I, Scenario-V, Scenario-V' and Scenario-IV, the lower bound on  $m_{Z'}$  is extracted to be about 1000 GeV, 800

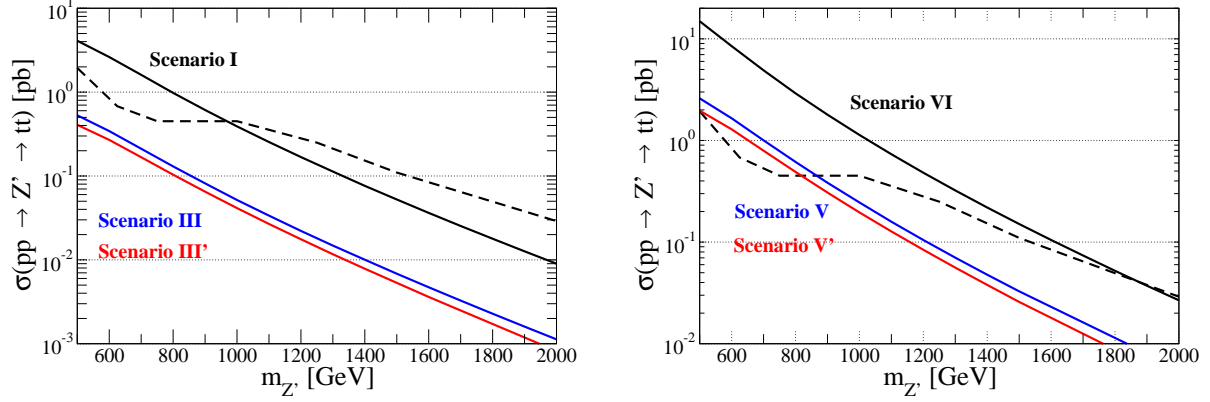


FIG. 4: Cross section of the  $pp \rightarrow Z' \rightarrow t\bar{t}$  process as a function of  $m_{Z'}$  for the collision energy of 8 TeV. The left (right) panel shows the results in Scenario-I, -III and -III' (-V, -V' and -VI). The dashed curve is the observed limit at the 95 % CL from the LHC data [21].

GeV, 850 GeV and 1900 GeV, respectively. On the other hand, no bound is obtained from this process in Scenario-III and Scenario-III'.

## B. The dijet process

Dijet events at hadron colliders are useful for the detection and property analysis of a leptophobic  $Z'$  boson as one can readily measure a peak in the dijet invariant mass and study their angular distribution. Using the dijet resonant events at the LHC, Ref. [22] put constraints on the mass and coupling constant for the leptophobic  $Z'$  boson. In Ref. [23], it had been shown that the angular distribution of the dijet events with a high invariant mass could be used to probe the mass scales associated with different dimension-6 operators by using an effective Lagrangian approach. In particular, of interest to us is that the dijet process can receive contributions from four-quark interactions mediated by a  $Z'$  boson when the  $Z'$  mass is taken to be much larger than the typical jet momentum. Such a new interaction term can modify the dijet distribution from that of the QCD prediction. Thus, using the experimental dijet events, one can constrain the  $Z'$  mass provided the coupling constant is fixed.

The dijet measurement had been done at the LHC, offering various distributions [24, 25]. In order to compare the dijet events including the  $Z'$  mediation with the experimental data, we define  $F_\chi$  value [24] as the ratio of two numbers of events in different regions of  $\chi$  as

$$F_\chi(m_{jj}^{\text{cut}}) \equiv \frac{N(\chi < 3.32, m_{jj}^{\text{cut}})}{N(\chi < 30.0, m_{jj}^{\text{cut}})}, \quad (4)$$



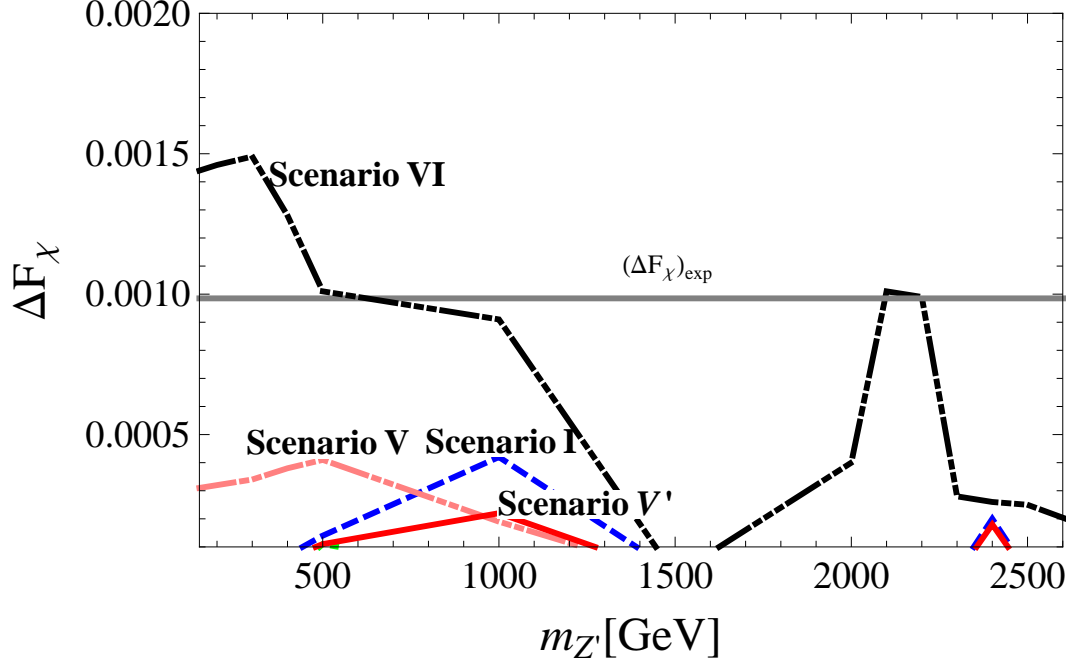


FIG. 5: Values of  $\Delta F_\chi$ , defined in the text, in the different scenarios. The horizontal line corresponds to the upper limit for  $\Delta F_\chi$  at 95% confidence level.

where  $\chi \equiv \exp(|y_1 - y_2|)$  with  $y_{1,2}$  being the jet rapidities, and  $m_{jj}^{\text{cut}}$  is the invariant mass cut for the dijet system. Ref. [25] provides the dijet event data with  $m_{jj}^{\text{cut}}$  as  $2 \text{ TeV} < m_{jj} < 2.6 \text{ TeV}$  based on the  $4.8 \text{ fb}^{-1}$  data at 7 TeV. The central value of  $F_\chi$  is extracted to be about 0.0848.

We directly calculate the deviation in the value of  $F_\chi$  from the SM prediction by using MADGRAPH [26] and CTEQ6L, instead of working with the effective Lagrangian. This is because the mass region considered here is not large enough compared to the dijet invariant mass. The deviation can be expressed as

$$\Delta F_\chi \equiv \text{MIN}|F_\chi^{Z'}(1 \pm 0.02) - F_\chi^{\text{SM}}(1 \pm 0.02)|, \quad (5)$$

where  $F_\chi^{Z'}$  and  $F_\chi^{\text{SM}}$  are respectively the values of  $F_\chi(m_{jj}^{\text{cut}})$  in the six scenarios of the leptophobic  $Z'$  and in the SM. In the numerical calculation, there is about 2% uncertainty in the cross section. We therefore insert the factor  $(1 \pm 0.02)$  and pick the minimum on the right hand side. When the SM prediction is assumed to be the same as the experimental central value, one can set a 95% CL upper limit on  $\Delta F_\chi$  by requiring  $\Delta F_\chi < 1.96/\sqrt{N_{\text{exp}}}$ , where  $N_{\text{exp}}$  ( $= 28462$ ) is the event number measured at the LHC [25].

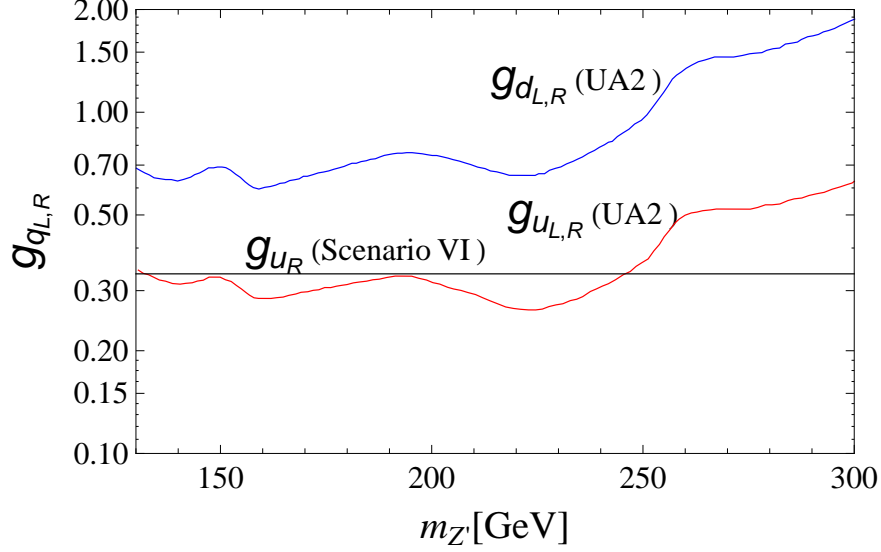


FIG. 6: Constraints on the  $Z'\bar{q}q$  couplings (blue curve for the down-type quarks and red curve for the up-type quarks) taken from Ref. [15] compared with  $g_{u_R}$  in Scenario-VI (black horizontal line).

In Fig. 5, we show values of  $\Delta F_\chi$  as a function of  $m_{Z'}$  in the six scenarios. The 95% CL upper limit for  $\Delta F_\chi$  is indicated by the horizontal line. As shown in this figure, a  $Z'$  with mass smaller than about 500 GeV is excluded only in Scenario-VI. On the other hand, no significant deviation in  $F_\chi$  can be found in all the other scenarios. The peak at around 2 TeV for Scenario-VI is due to our choice of the dijet invariant mass cut,  $2 \text{ TeV} \leq m_{jj} \leq 2.6 \text{ TeV}$ .

### C. The constraints from UA2

The  $Z'\bar{q}q$  couplings had been constrained using UA2 experimental measurements. In Ref. [15], the UA2 constraints are given for the coupling constants appearing in the following interaction

$$g_{q_{L,R}} \bar{q} \gamma^\mu \frac{1 \mp \gamma_5}{2} q Z'_\mu, \quad (6)$$

where  $q = u, d$ . These coupling constants are related to the variables in Eq. (1) by

$$g_{q_{L,R}} = g_{Z'}(v_q \pm a_q), \quad (7)$$

We find that the coupling constants are well below the UA2 constraints given in Fig. 1 of Ref. [15]. Only for  $g_{u_R}$  in Scenario-VI, the region  $m_{Z'} \lesssim 250 \text{ GeV}$  is excluded as shown in Fig. 6.

	Scenario-I	Scenario-III	Scenario-III'	Scenario-V	Scenario-V'	Scenario-VI
$pp \rightarrow t\bar{t}$	1000 GeV	-	-	800 GeV	850 GeV	1900 GeV
dijet	-	-	-	-	-	500 GeV
UA2	-	-	-	-	-	250 GeV

TABLE II: Lower bounds on  $m_{Z'}$  at 95% CL for all the scenarios by existing experiments.

#### D. Summary of constraint on $m_{Z'}$

Here we summarize the constraints on  $m_{Z'}$  discussed in this section. The lower bounds on  $m_{Z'}$  at 95% CL for all the scenarios are listed in Table II. The constraint from the  $pp \rightarrow t\bar{t}$  process is the strongest among all. However, this constraint can only be applied to the case where the  $Z' \rightarrow t\bar{t}$  decay is kinematically allowed. On the other hand, the constraints from the dijet events and the UA2 experiment can be applied to the lighter  $Z'$  case; namely,  $m_{Z'} < 2m_t$ . However, scenarios other than Scenario-VI are not restricted by these data either because of the small  $Z'$  charges for the up-type quarks. In the next section, we discuss such a light  $Z'$  case by using  $t$ -channel processes  $pp \rightarrow Z'V$ , where  $V = \gamma, Z$  and  $W$ . We will see that only the  $pp \rightarrow Z'\gamma$  process is useful in bounding the  $Z'$  mass.

### IV. SIMULATION STUDY OF A $t$ -CHANNEL PROCESS

In this section, we consider the  $t$ -channel process  $pp \rightarrow Z'\gamma \rightarrow b\bar{b}\gamma$  for a relatively light  $Z'$  with  $m_{Z'} \lesssim 350$  GeV where the  $Z' \rightarrow t\bar{t}$  decay is kinematically forbidden. Since no experimental data exist at the time of writing, we present a simulation study here. With  $b$ -tagging, the  $Z' \rightarrow b\bar{b}$  decay is expected to have higher sensitivity than the  $Z' \rightarrow q\bar{q}$  decays, where  $q$  refers to quarks in the first and second generations. For the backgrounds, we include the SM irreducible background  $pp \rightarrow b\bar{b}\gamma$  and the  $pp \rightarrow q\bar{q}\gamma$  process with mis-tagging of the  $b$  quarks.

We here comment on the other  $t$ -channel processes, *i.e.*,  $pp \rightarrow Z'W \rightarrow b\bar{b}W$  and  $pp \rightarrow Z'Z \rightarrow b\bar{b}Z$ . These cross sections are about one order of magnitude smaller than that of  $pp \rightarrow Z'\gamma$  as shown in Fig. 3. On the other hand, the background cross sections for the  $b\bar{b}W$  and  $b\bar{b}Z$  processes are estimated to be about 3-4 times smaller than that for  $\gamma b\bar{b}$ . In addition, if we take leptonic decays of the  $W$  and  $Z$  bosons, both signal and background cross sections are further decreased by one order of magnitude. Consequently, the signal significance of the  $pp \rightarrow Z'W$  and  $pp \rightarrow Z'Z$  modes are expected to be one order of magnitude smaller than that of  $pp \rightarrow Z'\gamma$ . We therefore do

	$\gamma Z'(\rightarrow b\bar{b})$	$\gamma b\bar{b}$	$\gamma jj$	$\mathcal{S}$
Basic cuts in Eq. (8)	0.256	21.8	2952	0.66
Double b-tagging	0.0269	2.39	3.60	1.54
$M_{b\bar{b}}$ cut in Eq. (9)	0.015	0.449	0.541	2.14

TABLE III: Cross sections of signal and background processes in Scenario-I in units of pb, assuming  $m_{Z'} = 200$  GeV and  $\sqrt{s} = 8$  TeV. To calculate the significance  $\mathcal{S}$ , we take an integrated luminosity of  $19.6 \text{ fb}^{-1}$ . The basic cuts Eq. (8) are imposed, and the double b-tagging is applied after detector simulations by PGS.

not consider these channels here.

In our analysis, we generate signal and background events using MADGRAPH/MADEVENT [26] and the CTEQ6L PDF's for the collision energies  $\sqrt{s} = 8$  TeV and 14 TeV. The generated events are passed onto PYTHIA [27] through the PYTHIA-PGS package to include initial-state radiation, final-state radiation and hadronization effects. The detector level simulation is then carried out by PGS [28]. When generating the events, we apply the following basic kinematical cuts:

$$\begin{aligned}
p_T(\text{jets}) &> 40 \text{ GeV}, \quad p_T(\gamma) > 10 \text{ GeV}, \\
|\eta(\text{jets})| &< 2.4, \quad |\Delta\eta_{jj}| < 2.4, \\
90 \text{ GeV} &< M_{jj} < 360 \text{ GeV},
\end{aligned} \tag{8}$$

where the jets include b-jets, and  $|\Delta\eta_{jj}|$  is the rapidity difference of the two jets. We impose double b-tagging after the PGS detector simulation to reduce the background events. Afterwards, we further take a cut on the invariant mass of the two b-jet system  $M_{b\bar{b}}$ :

$$m_{Z'}(1 - 0.2) < M_{b\bar{b}} < m_{Z'} + 10 \text{ GeV} \tag{9}$$

for each  $m_{Z'}$  value<sup>1</sup>. We also calculate the signal significance defined by [29]  $\mathcal{S} = \sqrt{2[(s+b)\ln(s/b) - s]}$ , where  $s$  and  $b$  are numbers of signal and background events, respectively. In Table. III, we show an example of how the cuts affect the number of events in Scenario-I, assuming  $m_{Z'} = 200$  GeV and  $\sqrt{s} = 8$  TeV. The  $\gamma jj$  background is significantly reduced by about three orders of magnitude by double b-tagging while the signal and irreducible background are down by one order of magnitude, thereby enhancing the significance by more than a factor of two. We also observe that the  $M_{b\bar{b}}$  cut is effective in reducing not only the  $\gamma jj$  background but also the irreducible background.

<sup>1</sup> Because the shape of the  $b\bar{b}$  invariant mass distribution is asymmetric around  $M_{b\bar{b}} = m_{Z'}$ , we use different upper and lower cut limits for  $M_{b\bar{b}}$  in Eq. (9).

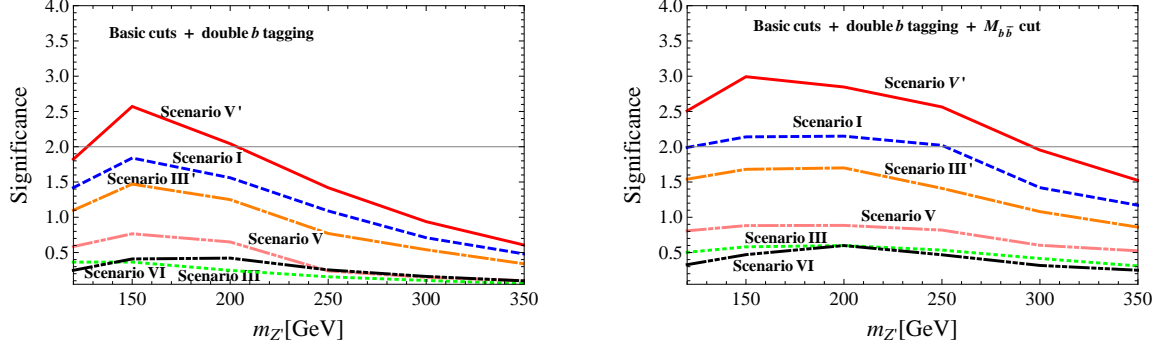


FIG. 7: Significance  $\mathcal{S}$  for the  $pp \rightarrow Z'\gamma \rightarrow b\bar{b}\gamma$  process at the LHC with  $\sqrt{s} = 8$  TeV and an integrated luminosity of  $19.6\text{fb}^{-1}$ . The left panel shows the result after imposing the basic cuts and double b-tagging, and right panel that after the  $M_{b\bar{b}}$  cut is also imposed.

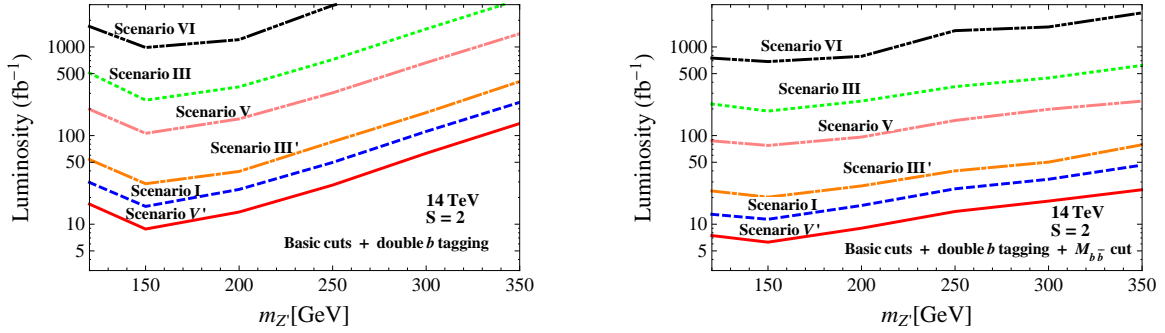


FIG. 8: Required integrated luminosity to obtain the significance  $\mathcal{S} = 2$  in the  $pp \rightarrow Z'\gamma \rightarrow b\bar{b}\gamma$  process at the LHC with  $\sqrt{s} = 14$  TeV. The left panel shows the result after imposing the basic cuts and double b-tagging, and right panel that after the  $M_{b\bar{b}}$  cut is also imposed.

In Fig. 7, we show the significance  $\mathcal{S}$  for the six scenarios as a function of  $m_{Z'}$ , assuming  $\sqrt{s} = 8$  TeV and an integrated luminosity of  $19.6\text{fb}^{-1}$ . The left panel shows the result after the basic cuts and double b-tagging, and the right panel that after the  $M_{b\bar{b}}$  cut is also imposed. We find that the mass range of  $130\text{ GeV} \lesssim m_{Z'} \lesssim 200\text{ GeV}$  is excluded at 95% CL for Scenario-V' using the basic cuts and double b-tagging. After further imposing the  $M_{b\bar{b}}$  cut, the mass range of  $120\text{ GeV} \lesssim m_{Z'} \lesssim 290$  (240) GeV can be excluded for Scenario-V' (Scenario-I) at 95% CL. The other scenarios will be less constrained by this analysis. The hierarchy in the significances of the different scenarios depends on the product of the cross section of  $pp \rightarrow Z'\gamma$ , shown in Fig. 3, and the branching fraction of  $Z' \rightarrow b\bar{b}$ , given in Table. I.

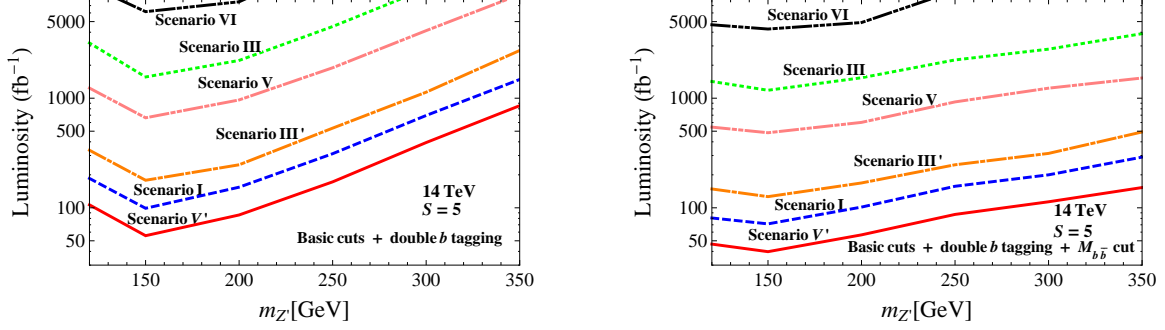


FIG. 9: Same as Fig. 8, but for  $S = 5$ .

In Fig. 8, the required integrated luminosity to reach  $S = 2$  is shown as a function of  $m_{Z'}$  in the case of  $\sqrt{s} = 14$  TeV. The left panel shows the results after imposing the basic cuts and double b-tagging. The  $M_{b\bar{b}}$  cut is further imposed to produce the plot in the right panel. The result for the required integrated luminosity to reach  $S = 5$  is given in Fig. 9.

We thus find that the significance of 2 (5) can be obtained with an integrated luminosity of  $100 \text{ fb}^{-1}$  in Scenario-V' with  $m_{Z'} \lesssim 340$  (200) GeV, in Scenario-I with  $m_{Z'} \lesssim 300$  (-) GeV, and in Scenario-III' with  $m_{Z'} \lesssim 270$  (-) GeV by using only the basic cuts and double b-tagging. Applying further the  $M_{b\bar{b}}$  cut, the significance of 2 (5) can be obtained with an integrated luminosity of  $100 \text{ fb}^{-1}$  in Scenario-V' with  $m_{Z'} \lesssim 350$  (290) GeV, in Scenario-I with  $m_{Z'} \lesssim 350$  (190) GeV, in Scenario-III' with  $m_{Z'} \lesssim 350$  (-) GeV, and in Scenario-V with  $m_{Z'} \lesssim 200$  (-) GeV. If we assume an integrated luminosity of  $500 \text{ fb}^{-1}$ , all the scenarios excepted for Scenario-VI can reach  $S = 2$  within the mass range shown in the figures (*i.e.*, between 120 and 350 GeV) after imposing the basic cuts, double b-tagging and  $M_{b\bar{b}}$  cut. Using the same kinematic cuts, the 5-sigma discovery can be obtained in Scenario-I, Scenario-III' and Scenario-V'. In the other scenarios, more than  $500 \text{ fb}^{-1}$  is needed to achieve a 5-sigma discovery in certain mass ranges.

Finally, we would like to comment on the search for the leptophobic  $Z'$  boson at the international linear collider (ILC)<sup>2</sup>. Even though the ILC is an electron-positron collider where the initial leptons do not couple to a leptophobic  $Z'$  boson, it can still be produced in association with the quark pair production, *i.e.*,  $e^+e^- \rightarrow \gamma^*/Z^* \rightarrow q\bar{q}Z'$ . There are several designs of the ILC collision energy, namely, 250 GeV, 350 GeV and 500 GeV. Therefore, the  $Z'$  boson with a mass smaller

<sup>2</sup> Recently, phenomenology of  $Z'$  at the ILC has been discussed in Ref. [30] in a model-independent way using the  $e^+e^- \rightarrow \mu^+\mu^-/\tau^+\tau^-$  process.

than these energies can be produced in association with light quark pairs<sup>3</sup>. In particular, it would be interesting to analyze the case with  $m_{Z'} < 2m_t$  as it is difficult to probe using the current experimental data as we have shown in the previous section. This will lead to the signal of four hard jets with the invariant mass of two sitting at the  $Z'$  mass. For example, the cross section of  $e^+e^- \rightarrow q\bar{q}Z'$  with  $m_{Z'} = 150$  GeV at a 250-GeV ILC is estimated to be 0.1 fb. If such a  $Z'$  is discovered in the 14-TeV run of LHC, one may use the above-mentioned process to study detailed properties of the new boson. Even in the case where such a boson is not found at the LHC and the exclusion limit has not reached the 95% CL, one can use this process as a discovery channel. In any case, it is important to prepare the simulation study for the  $Z'$  boson at the ILC. A detailed analysis for leptophobic  $Z'$  searches at the ILC will be presented in a separate work [31].

## V. CONCLUSIONS

We have studied the phenomenology of a leptophobic  $Z'$  boson that can be naturally derived from the  $E_6$  GUT model, as a result of kinetic mixing between  $U(1)_Y$  and the extra  $U(1)$  symmetries. Due to different embedding schemes for the matter fields in the  $E_6$  fundamental representation, there are eight possible scenarios with a leptophobic  $Z'$ , differing in the  $Z'$  charges for the quarks. Three of the scenarios have the same  $Z'$  charge ratios. Therefore, the production cross sections of these scenarios can be related to one another by simple scaling. This reduces the number of distinct scenarios to six.

We have taken into account various experimental data to constrain the  $Z'$  mass, including the  $pp \rightarrow t\bar{t}$ , the dijet events and the UA2 data. The strongest bound on the  $Z'$  mass comes from the  $pp \rightarrow t\bar{t}$  process when  $Z' \rightarrow t\bar{t}$  is kinematically allowed. The lower limits at 95% confidence level are about 1 TeV, 0.8 TeV, 0.85 GeV and 1.9 TeV in Scenario-I, Scenario-V, Scenario-V' and Scenario-VI, respectively. However, this process is not effective when  $m_{Z'} < 2m_t$ .

We have then investigated the photon associated production of the  $Z'$  boson followed by the decay into a pair of bottom quarks, *i.e.*,  $pp \rightarrow \gamma Z' \rightarrow \gamma b\bar{b}$  in the lower mass region. We have found that Scenario-I (usually called the standard  $E_6$ ) with  $m_{Z'} \lesssim 250$  GeV can be excluded at 95% confidence level using the current LHC  $19.6 \text{ fb}^{-1}$  data at 8 TeV. A similar bound of  $m_{Z'} \lesssim 300$  GeV has also been obtained for Scenario-V'. Assuming an integrated luminosity of  $100 \text{ fb}^{-1}$  at the 14-TeV LHC, a significance over 2 can be obtained for  $m_{Z'} \lesssim 350$  GeV in Scenario-I, Scenario-III'

---

<sup>3</sup> Although one can consider the  $e^+e^- \rightarrow t\bar{t}Z'$  process, it suffers from a kinematic disadvantage.

and Scenario-V' after taking the basic cuts, double b-tagging and  $M_{b\bar{b}}$  cut. In the same setup, a significance of 5 can be obtained for  $m_{Z'} \lesssim 290$  GeV in Scenario-V' and  $m_{Z'} \lesssim 190$  GeV in Scenario-I.

### Acknowledgments

C.-W. C would like to thank D. Choudhury and N. Gaur for useful discussions during the very early stage of this project. This research was supported in part by the National Science Council of R. O. C. under Grant Nos. NSC-100-2628-M-008-003-MY4, NSC-101-2811-M-008-014 and NSC-102-2811-M-006-035.

### APPENDIX: Review of $E_6$ GUT model

We present a brief review of scenarios in the  $E_6$  GUT model that predict a leptophobic  $Z'$  boson, with its detailed derivations and fermion interactions given in Ref. [19]. The symmetry breaking of  $E_6$  follows the pattern of

$$E_6 \rightarrow SO(10) \times U(1)_\psi \rightarrow SU(5) \times U(1)_\chi \times U(1)_\psi \rightarrow G_{\text{SM}} \times U(1)_{Q'} . \quad (10)$$

The  $U(1)_{Q'}$  symmetry is obtained as a linear combination of  $U(1)_\psi$  and  $U(1)_\chi$ , with the corresponding charge expressed as

$$Q' = Q_\psi \cos \theta - Q_\chi \sin \theta, \quad (11)$$

where  $Q_\psi$  and  $Q_\chi$  are the charges under  $U(1)_\psi$  and  $U(1)_\chi$ , respectively.

The most general kinetic terms, including kinetic mixing, for the gauge fields and interaction terms for a fermion  $\psi$  are given as

$$\mathcal{L}_{\text{kin}} = -\frac{1}{4}W_{\mu\nu}^a W^{a\mu\nu} - \frac{1}{4}(\tilde{B}_{\mu\nu}, \tilde{Z}'_{\mu\nu}) \begin{pmatrix} 1 & \sin \chi \\ \sin \chi & 1 \end{pmatrix} \begin{pmatrix} \tilde{B}^{\mu\nu} \\ \tilde{Z}'^{\mu\nu} \end{pmatrix}, \quad (12)$$

$$\mathcal{L}_{\text{int}} = -\bar{\psi}\gamma^\mu (gT^a W_\mu^a + g'Y\tilde{B}_\mu + \tilde{g}_{Z'}Q'\tilde{Z}'_\mu)\psi, \quad (13)$$

where  $g$  and  $g'$  are the SM  $SU(2)_L$  and  $U(1)_Y$  gauge couplings, and  $Y$  is the SM  $U(1)_Y$  hypercharge<sup>4</sup>. Through a non-unitary transformation,

$$\begin{pmatrix} \tilde{B}_\mu \\ \tilde{Z}'_\mu \end{pmatrix} = \begin{pmatrix} 1 & -\tan \chi \\ 0 & \sec \chi \end{pmatrix} \begin{pmatrix} B_\mu \\ Z'_\mu \end{pmatrix}, \quad (14)$$

---

<sup>4</sup> We do not pull out the factors of  $\sqrt{3/5}$  and  $\sqrt{5/3}$  for  $Y$  and  $g'$ , respectively.



the gauge fields  $\tilde{Z}'_\mu$  and  $\tilde{B}_\mu$  are diagonalized to the fields  $Z'_\mu$  and  $B_\mu$  of mass eigenstates. The interaction terms are then rewritten as

$$\mathcal{L}_{\text{int}} = -\bar{\psi}\gamma^\mu(gT^a W_\mu^a + g'Y B_\mu + g_{Z'}\bar{Q}Z'_\mu)\psi, \quad (15)$$

where  $g_{Z'} \equiv \tilde{g}_{Z'}/\cos\chi$ , and the  $Z'$  charge  $\bar{Q}$  for a fermion field  $f$  is

$$\bar{Q}(f) \equiv Q'(f) + \sqrt{\frac{3}{5}}\delta Y, \quad \text{with } \delta \equiv -\sqrt{\frac{5}{3}}\frac{g'}{g_{Z'}}\tan\chi. \quad (16)$$

As is evident in Eq. (16), all  $\bar{Q}(f)$  charges are determined by two unknown parameters; *i.e.*,  $\theta$  and  $\delta$ . This implies that once we fix two of  $\bar{Q}(f)$  charges, all the other  $\bar{Q}(f)$  charges are uniquely determined as well. We utilize this feature to find scenarios with a leptophobic  $Z'$ ; that is,

$$\bar{Q}(L) = Q'(L) - \frac{1}{2}\delta = 0, \quad \bar{Q}(e^c) = Q'(e^c) + \delta = 0. \quad (17)$$

These two equations are solved to render

$$\tan\theta = \frac{2Q_\psi(L) + Q_\psi(e^c)}{2Q_\chi(L) + Q_\chi(e^c)}, \quad \delta = -Q'(e^c) (= 2Q'(L)). \quad (18)$$

There are then six ways to embed the SM fermions, along with new fermions, into the **27** representation of  $E_6$ . In Table IV,  $U(1)$  charges of the fermions are listed for the six scenarios, following the convention of Ref. [18]. In this table, only  $h^c$  is a non-SM fermion whose SM gauge quantum numbers are the same as those of  $d^c$ . Thus, one can interchange the  $U(1)_\psi$  and  $U(1)_\chi$  charges of  $d^c$  with those of  $h^c$ . After the interchange, the  $Q'$  and  $\bar{Q}$  charges of  $d^c$  and  $h^c$  are different from the original ones only in Scenario-III and Scenario-V. We denote the two new scenarios by Scenario-III' and Scenario-V', respectively.

- 
- [1] G. Aad *et al.* [ATLAS Collaboration], Phys. Lett. B **716**, 1 (2012); S. Chatrchyan *et al.* [CMS Collaboration], Phys. Lett. B **716**, 30 (2012).
  - [2] E. Ma, Phys. Rev. D **36**, 274 (1987); K. S. Babu, X. -G. He and E. Ma, Phys. Rev. D **36**, 878 (1987); F. Zwirner, Int. J. Mod. Phys. A **3**, 49 (1988); J. L. Hewett and T. G. Rizzo, Phys. Rept. **183**, 193 (1989); Y. Daikoku and H. Okada, Phys. Rev. D **82**, 033007 (2010) [arXiv:0910.3370 [hep-ph]].
  - [3] L. M. Krauss and F. Wilczek, Phys. Rev. Lett. **62**, 1221 (1989); J. Kubo and D. Suematsu, Phys. Lett. B **643**, 336 (2006) [hep-ph/0610006].
  - [4] S. Kanemura, O. Seto and T. Shimomura, Phys. Rev. D **84**, 016004 (2011) [arXiv:1101.5713 [hep-ph]]; S. Kanemura, T. Nabeshima and H. Sugiyama, Phys. Rev. D **85**, 033004 (2012) [arXiv:1111.0599 [hep-ph]]; C. -W. Chiang, T. Nomura and J. Tandean, Phys. Rev. D **87**, no. 7, 073004 (2013)

	Scenario-I				Scenario-II				Scenario-III (Scenario-III')			
	$\tan \theta = \sqrt{3/5}, \delta = -1/3$				$\tan \theta = \sqrt{15}, \delta = -\sqrt{10}/3$				$\tan \theta = \sqrt{5/3}, \delta = -\sqrt{5/12}$			
	$2\sqrt{6}Q_\psi$	$2\sqrt{10}Q_\chi$	$\sqrt{15}Q'$	$\sqrt{15}\bar{Q}$	$2\sqrt{6}Q_\psi$	$2\sqrt{10}Q_\chi$	$\sqrt{6}Q'$	$\sqrt{6}\bar{Q}$	$2\sqrt{6}Q_\psi$	$2\sqrt{10}Q_\chi$	$Q'$	$\bar{Q}$
$Q$	1	-1	1	5/6	1	-1	1/2	1/6	1	-1	1/4	1/6
$u^c$	1	-1	1	5/3	1	3	-1	1/3	1	3	-1/4	1/12
$d^c$	1	3	-1/2	-5/6	1	-1	1/2	-1/6	1 (1)	-1 (3)	1/4 (-1/4)	1/12 (-5/12)
$h^c$	-2	-2	-1/2	-5/6	-2	-2	1/2	-1/6	1 (1)	3 (-1)	-1/4 (1/4)	-5/12 (1/12)
$L$	1	3	-1/2	0	1	3	-1	0	1	3	-1/4	0
$e^c$	1	-1	1	0	1	-5	2	0	4	0	1/2	0

	Scenario-IV				Scenario-V (Scenario-V')				Scenario-VI			
	$\tan \theta = \sqrt{3/5}, \delta = -1/3$				$\tan \theta = \sqrt{5/27}, \delta = -\sqrt{5/12}$				$\tan \theta = 0, \delta = -\sqrt{10}/3$			
	$2\sqrt{6}Q_\psi$	$2\sqrt{10}Q_\chi$	$\sqrt{15}Q'$	$\sqrt{15}\bar{Q}$	$2\sqrt{6}Q_\psi$	$2\sqrt{10}Q_\chi$	$Q'$	$\bar{Q}$	$2\sqrt{6}Q_\psi$	$2\sqrt{10}Q_\chi$	$\sqrt{6}Q'$	$\sqrt{6}\bar{Q}$
$Q$	1	-1	1	5/6	1	-1	1/4	1/6	1	-1	1/2	1/6
$u^c$	1	-1	1	5/3	1	3	0	1/3	1	3	1/2	11/6
$d^c$	1	3	-1/2	-5/6	1 (-2)	-1 (-2)	1/4 (-1/4)	1/12 (-5/12)	1	-1	1/2	-1/6
$h^c$	-2	-2	-1/2	-5/6	-2 (1)	-2 (-1)	-1/4 (1/4)	-5/12 (1/12)	1	3	1/2	-1/6
$L$	-2	-2	-1/2	0	-2	-2	-1/4	0	-2	-2	-1	0
$e^c$	1	-1	1	0	1	-5	1/2	0	4	0	2	0

TABLE IV:  $U(1)$  charges of six leptophobic scenarios in the  $E_6$  GUT model. In the last row,  $h^c$  denotes a non-SM fermion in the fundamental representation of  $E_6$ .

- [arXiv:1205.6416 [hep-ph]]; S. Kanemura, T. Nabeshima and H. Sugiyama, Phys. Rev. D **87**, 015009 (2013) [arXiv:1207.7061 [hep-ph]].
- [5] Y. Daikoku, H. Okada and T. Toma, Prog. Theor. Phys. **126**, 855 (2011) [arXiv:1106.4717 [hep-ph]]; Y. Daikoku and H. Okada, Phys. Rev. D **88**, 015034 (2013) [arXiv:1303.7056 [hep-ph]].
- [6] S. W. Ham, E. J. Yoo and S. K. Oh, Phys. Rev. D **76**, 015004 (2007) [hep-ph/0703041 [hep-ph]]; S. W. Ham, E. J. Yoo and S. K. OH, Phys. Rev. D **76**, 075011 (2007) [arXiv:0704.0328 [hep-ph]]; C. -W. Chiang and E. Senaha, JHEP **1006**, 030 (2010) [arXiv:0912.5069 [hep-ph]]; A. Ahriche and S. Nasri, Phys. Rev. D **83**, 045032 (2011) [arXiv:1008.3106 [hep-ph]]; E. Senaha, Phys. Rev. D **88**, 055014 (2013) [arXiv:1308.3389 [hep-ph]].
- [7] V. A. Kuzmin, V. A. Rubakov and M. E. Shaposhnikov, Phys. Lett. B **155**, 36 (1985).
- [8] For nice and comprehensive reviews on  $Z'$  phenomenology in various models, please see, for example, P. Langacker, Rev. Mod. Phys. **81**, 1199 (2009) [arXiv:0801.1345 [hep-ph]]; P. Langacker and M. Plumacher, Phys. Rev. D **62**, 013006 (2000) [hep-ph/0001204].

- [9] ATLAS-CONF-2013-017
- [10] ATLAS-CONF-2013-066
- [11] K. S. Babu, C. F. Kolda and J. March-Russell, Phys. Rev. D **54**, 4635 (1996) [hep-ph/9603212]; K. S. Babu, C. F. Kolda and J. March-Russell, Phys. Rev. D **57**, 6788 (1998) [hep-ph/9710441].
- [12] V. D. Barger, K. -m. Cheung and P. Langacker, Phys. Lett. B **381**, 226 (1996) [hep-ph/9604298].
- [13] M. Heyssler, Phys. Rev. D **54**, 5845 (1996) [hep-ph/9605403]; F. del Aguila and J. A. Aguilar-Saavedra, JHEP **0711**, 072 (2007) [arXiv:0705.4117 [hep-ph]]; V. Barger, P. Langacker and H. -S. Lee, Phys. Rev. Lett. **103**, 251802 (2009) [arXiv:0909.2641 [hep-ph]].
- [14] H. An, R. Huo and L. -T. Wang, Phys. Dark Univ. **2**, 50 (2013) [arXiv:1212.2221 [hep-ph]]; A. Alves, S. Profumo and F. S. Queiroz, arXiv:1312.5281 [hep-ph].
- [15] M. R. Buckley, D. Hooper, J. Kopp and E. Neil, Phys. Rev. D **83**, 115013 (2011) [arXiv:1103.6035 [hep-ph]].
- [16] K. Cheung and J. Song, Phys. Rev. Lett. **106**, 211803 (2011) [arXiv:1104.1375 [hep-ph]]; K. Cheung and J. Song, Phys. Rev. D **84**, 034043 (2011) [arXiv:1106.6141 [hep-ph]].
- [17] Y. Umeda, G. -C. Cho and K. Hagiwara, Phys. Rev. D **58**, 115008 (1998) [hep-ph/9805447]; G. -C. Cho, K. Hagiwara and Y. Umeda, Nucl. Phys. B **531**, 65 (1998) [Erratum-ibid. B **555**, 651 (1999)] [hep-ph/9805448]; M. R. Buckley and M. J. Ramsey-Musolf, Phys. Lett. B **712**, 261 (2012) [arXiv:1203.1102 [hep-ph]]; M. González-Alonso and M. J. Ramsey-Musolf, Phys. Rev. D **87**, no. 5, 055013 (2013) [arXiv:1211.4581 [hep-ph]].
- [18] K. Leroux and D. London, Phys. Lett. B **526**, 97 (2002) [hep-ph/0111246].
- [19] T. G. Rizzo, Phys. Rev. D **59**, 015020 (1998) [hep-ph/9806397].
- [20] A. Pukhov, [hep-ph/0412191].
- [21] CMS Collaboration, CMS PAS B2G-12-006 (2013).
- [22] B. A. Dobrescu and F. Yu, Phys. Rev. D **88**, 035021 (2013) [arXiv:1306.2629 [hep-ph]].
- [23] O. Domenech, A. Pomarol, J. Serra, Phys. Rev. D **85**, 074030 (2012) [arXiv:1201.6510].
- [24] G. Aad *et al.* [ATLAS Collaboration], New J. Phys. **13**, 053044 (2011) [arXiv:1103.3864 [hep-ex]].
- [25] G. Aad *et al.* [ATLAS Collaboration], JHEP **1301**, 029 (2013) [arXiv:1210.1718 [hep-ex]].
- [26] J. Alwall, M. Herquet, F. Maltoni, O. Mattelaer and T. Stelzer, JHEP **1106**, 128 (2011) [arXiv:1106.0522 [hep-ph]].
- [27] T. Sjostrand, S. Mrenna, P. Z. Skands, JHEP **0605**, 026 (2006).
- [28] <http://www.physics.ucdavis.edu/conway/research/software/pgs/pgs4-general.htm>.
- [29] The CMS Collaboration J. Phys. G **34**, 995 (2007).
- [30] V. Skalozub and I. Kucher, arXiv:1402.1187 [hep-ph].
- [31] C. -W. Chiang, T. Nomura and K. Yagyu, work in preparation.